

## Porphyrins as ITO photosensitizers: substituents control photo-induced electron transfer direction†

Yulia Furmansky,<sup>ab</sup> Hela Sasson,<sup>ab</sup> Paul Liddell,<sup>c</sup> Devens Gust,<sup>c</sup> Nurit Ashkenasy<sup>db</sup> and Iris Visoly-Fisher<sup>\*ab</sup>

Received 25th June 2012, Accepted 6th August 2012

DOI: 10.1039/c2jm34118b

Porphyrins have attracted much attention as dyes for photovoltaic applications due to their remarkable light harvesting properties and tunability of electronic behaviour. The photophysical and photochemical properties of porphyrins are influenced by electron-donating or electron-withdrawing substituents that can be attached at the perimeter of the porphyrin macrocycle. The current work shows that changing the porphyrin peripheral substituents can affect the direction of interfacial charge transfer at the interface of porphyrin and Indium tin oxide (ITO), a degenerate n-type semiconductor that is commonly used as a transparent conductive electrode in organic optoelectronic devices. Soret-band excitation resulted in electron injection from the molecular layer to the ITO in all porphyrin derivatives studied, suggesting that electron injection to ITO is faster than relaxation from the porphyrin upper excited state to the lower one. However, the direction of photo-induced electron transfer in the 500–650 nm spectral range (Q-bands excitation in porphyrins) was found to depend on the peripheral substituents. This is highly relevant for photovoltaic devices, as the solar spectrum peaks in this spectral range. The charge transfer behaviour was shown to depend on the composition of the interfacial adsorbed monolayer. Therefore, it is proposed that porphyrin derivatives can be used for modulating photo-induced interfacial transport at ITO/organic layer interfaces in a predefined, controllable way.

## Introduction

Using organic materials as components of optoelectronic devices is aimed at exploiting their structural and mechanical flexibility, low weight and low cost, while reducing the environmental impact of production and operation.<sup>1–3</sup> Among the many factors limiting the performance of organic photovoltaic (OPV) devices, the efficiency of charge carrier injection at the interfaces between the photoactive layer and the electrodes is a central issue.<sup>4</sup> Modification of an inorganic electrode's surface by attachment of organic molecules is a promising way to improve the efficiency by modulating the interfacial energetics at the heterojunction, utilizing the molecular structural versatility for fine tuning of the interface energetics.<sup>5–10</sup> An adsorbed molecular monolayer can affect semiconductor surface electronic properties by changing the surface electron affinity<sup>5,11</sup> or/and the net surface-charge

density.<sup>12,13</sup> Recently, interfacial modification of TiO<sub>2</sub>/polymer interfaces in OPV devices by adsorption of photo-active dyes, including Ru-based, indoline-based and phthalocyanine-based dyes, was shown to improve the energy conversion efficiencies of the devices.<sup>14–17</sup> Herein we describe a study of charge injection at the interface between Indium tin oxide (ITO) and different porphyrin derivatives aimed at understanding the effect of substituents on such charge injection. Such understanding will allow both optimizing the use of porphyrins in molecular OPV devices, as well as evaluating the potential of porphyrins as photo-active interfacial modifiers in ITO/polymer devices.

Porphyrins have attracted much attention as dyes for photovoltaic applications due to their remarkable light harvesting properties and tunability of electronic behaviour.<sup>18–21</sup> Porphyrin-type compounds are frequently found in nature as part of the photosynthetic mechanism. The photophysical and photochemical properties of porphyrins are influenced by electron-donating or electron-withdrawing substituents that can be attached at the perimeter of the porphyrin macrocycle at the meso- or beta-positions.<sup>22</sup> For example, pyridyl meso-substituents were found to decrease the reduction potential of the porphyrin resulting in n-type conductance in solid porphyrin films.<sup>23</sup> The effect of different substituents has been widely studied in porphyrin-based dye sensitized solar cells.<sup>24,25</sup> Charge injection into TiO<sub>2</sub> electrodes was found to be strongly influenced by the nature of the binding group,<sup>26</sup> attachment of donor-acceptor

<sup>a</sup>Department of Chemistry, Ben Gurion University of the Negev, Be'er Sheva, Israel. E-mail: irisvf@bgu.ac.il; Fax: +972-8-6472943; Tel: +972-8-6472716

<sup>b</sup>Ilse Katz Institute for Nanoscale Science and Technology, Ben Gurion University of the Negev, Be'er Sheva, Israel

<sup>c</sup>Department of Chemistry and Biochemistry, Arizona State University, Tempe, AZ, USA

<sup>d</sup>Department of Materials Engineering, Ben Gurion University of the Negev, Be'er Sheva, Israel

† Electronic supplementary information available: Fig. S1–S4 and Tables S1–S3. See DOI: 10.1039/c2jm34118b

substituents<sup>25,27</sup> and the nature of spacer between the porphyrin macrocycle and anchoring functionality.<sup>28</sup> Dye-sensitized solar cells using porphyrins with an electron-donating meso-substituent and an electron-withdrawing anchoring group at the opposite meso-position have achieved record energy conversion efficiencies.<sup>24,25</sup> ITO is a degenerate n-type semiconductor with a large bandgap (3.75–4.1 eV)<sup>29,30</sup> which is commonly used as a transparent conductive oxide electrode in OPV devices due to its electronic conductivity and optical transparency. Tin oxide nanoparticles were also studied as an alternative or addition to the more commonly used TiO<sub>2</sub> electrode in dye sensitized solar cells due to their improved conductivity and electron mobility.<sup>18</sup> Surface and interface electronic properties of ITO can be significantly altered by the adsorption of a molecular monolayer,<sup>29,31</sup> and such treatments were used to improve the performance of organic PV and electro-optical devices utilizing ITO or ZnO as the transparent electrode.<sup>32–34</sup>

Surface photovoltage spectroscopy (SPS) is a contactless, non-destructive and sensitive tool for measuring illumination-induced electronic potential changes and charge redistribution at semiconductor surfaces and heterojunctions.<sup>37</sup> SPS was previously employed to characterize the photovoltage induced at various metal oxide/porphyrin film interfaces.<sup>35–39</sup> Though porphyrins are expected to donate electrons from their excited state to metal oxide electrode, in certain porphyrins an opposite direction of charge transfer was found upon excitation at the porphyrin Q-band absorption.<sup>37–39</sup> Specifically, such behaviour was observed at a porphyrin-C60 dyad/TiO<sub>2</sub> interface.<sup>37</sup> The direction and magnitude of photovoltage was found to depend also on the central substituent (metal or hydrogen atoms) of the porphyrin molecule.<sup>35,37</sup> However, to the best of our knowledge, no systematic study of the effect of porphyrin peripheral substituents on photo-induced charge transfer at interfaces with metal oxide electrodes has been performed hitherto. Here we report the investigation of the effect of porphyrin substituents on photo-induced charge transfer direction at porphyrin/ITO heterojunctions. SPS characterization shows that modifying the porphyrin macrocycle's periphery strongly affects the direction of photo-generated interfacial charge transfer, due to changes in energy level alignment and/or changes in the orientation of the molecules at the interface. Our results show that an interfacial porphyrin monolayer can tailor the electronic properties of the interface between photoactive organic films and ITO, controlling interfacial photo-induced charge transfer.

## Results and discussion

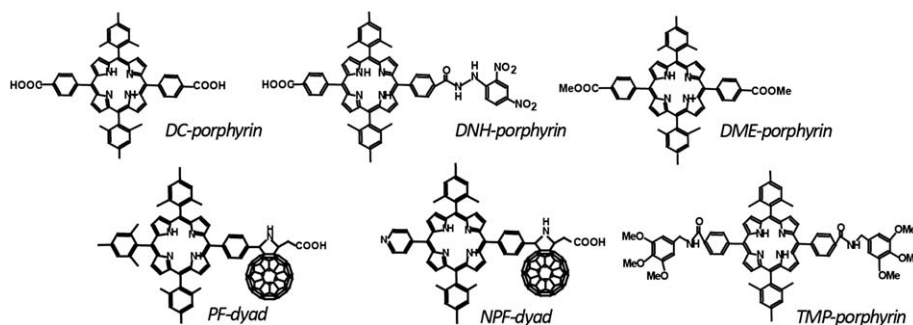
### Absorption, adsorption and cyclic voltammetry

The schematic molecular structures of the six differently substituted free-base tetraphenylporphyrins used in this study are presented in Scheme 1. The substituents were chosen in order to study the effect of electron donating or accepting substituents. Four types of porphyrins modified with carboxylic acid functionalities were chemically adsorbed on ITO surfaces: **DC-porphyrin** and **DNH-porphyrin**, both modified with a benzoic acid group at the 5-meso-position, differ by their 15-meso-position substituents: the second benzoic acid in **DC-porphyrin** can act both as an electron accepting group and as a second

anchoring group, while the phenyl-4-carboxy-(2,4-dinitrophenyl hydrazine) group in **DNH-porphyrin** has an increased electron-donating nature. The other two chemically adsorbed species are porphyrin–fullerene dyads (**PF-dyad** and **NPF-dyad**), where C60 is a strong electron acceptor. Such dyads showed quantitative yields of charge-separated species and long lifetimes of the charge-separated states when measured in solution.<sup>18,40</sup> In both **PF-dyad** and **NPF-dyad** the fullerene moiety is attached at the 5-meso-position *via* a conjugated phenyl spacer. In the **NPF-dyad** the mesityl group at the 15-meso-position was replaced by a pyridine ring as an electron-withdrawing substituent.<sup>41</sup> **DME-** and **TMP-porphyrins** were used for the formation of physically adsorbed multilayers on ITO substrates modified by monolayers of chemically adsorbed porphyrin derivatives (see below).

UV-Vis spectra of the adsorbed monolayers on ITO show the Soret band to be somewhat broader and red-shifted (1–2 nm) compared to that in solution (Fig. 1a compared to Fig. S1 and Table S1 in the ESI†). The lack of larger shifts rules out aggregation in the adsorbed films, probably due to the presence of bulky substituents.<sup>42,43</sup> The adsorption density in monolayers was estimated from the Soret absorption peak height and extinction coefficients measured in solution, and was found to be  $0.4 \pm 0.2 \times 10^{-10}$  mol cm<sup>-2</sup> in all monolayers. In multilayers (10–100 nm thick), the Soret absorption peaks of all porphyrins except for **TMP-porphyrin** further broadened and red shifted by 10–15 nm relative to those in solution, indicating interactions with the polar substrate and/or partial edge-on-edge J-type aggregation (Fig. 1b and Table S1†).<sup>44,45</sup> Absorption spectra of the porphyrin derivatives in solution show a Soret band absorption peak near 420 nm and four Q-bands at 517, 553, 593 and 650 nm (Fig. S1†), in accordance with typical values reported for free-base porphyrins.<sup>45,46</sup> Negligible differences in peak position and shape among the various porphyrins point to weak electronic interactions between the porphyrins and the attached substituents in the ground state.<sup>45,47</sup>

Cyclic voltammetry was carried out to determine the redox potentials of the chemically adsorbing porphyrins. Cathodic shifts of the first oxidation and reduction potentials in **DNH-porphyrin** compared to **DC-porphyrin** result from the electron-donating nature of the attached 2,4-dinitrophenyl hydrazine group. The relative anodic shifts of the redox potentials of the **NPF-dyad** compared to **PF-dyad** confirm the electron-withdrawing nature of the pyridine ring (Table S2†). The small shifts are another indication of the weak electronic interactions between the porphyrin and its substituents, as noted from the absorption spectra. In porphyrin–fullerene dyads, an additional transition indicates the reduction of the fullerene moiety. The molecular highest occupied molecular orbital (HOMO) and lowest unoccupied molecular orbital (LUMO) energies, at the electron energy scale, were estimated from the porphyrins' oxidation and reduction potentials, respectively, using a conversion value of –5.39 eV relative to the Fe/Fe<sup>+</sup> scale.<sup>48</sup> The estimated energy levels of the molecular orbitals are depicted in Scheme 2, together with the energies of the porphyrin excited states, calculated using excitation energies obtained from the absorption spectra,<sup>25,49,50</sup> and the measured Fermi level energies of bare ITO and ITO modified by thick multilayers of the four porphyrin derivatives. The latter were determined using the Kelvin probe technique.



Scheme 1 Schematic structures of porphyrin derivatives used in this study.

### Surface photovoltage spectroscopy (SPS)

SPS was used to study photo-induced charge transfer processes at the porphyrin/ITO interfaces.<sup>13,37,51</sup> Fig. 2 shows the surface photovoltage (SPV) as a function of the illuminating wavelength obtained from ITO samples modified by multilayer films of various porphyrin derivatives. SPV is the difference in the measured contact potential difference (CPD = sample work function – probe work function) in the dark and under illumination, *i.e.*,  $SPV = -(CPD_{\text{light}} - CPD_{\text{dark}})$ . A decrease in CPD upon illumination (increased SPV) indicates a decrease in the surface work function, corresponding to positive charging of the surface, and *vice versa*. The samples were illuminated through the transparent substrate. This configuration enhanced the measurement sensitivity to the interface of interest, *i.e.*, the porphyrin–ITO interface.<sup>35,36,38,39,52</sup> Photovoltage dependence on

the molecular layer thickness was previously noted when multilayers were illuminated through the porphyrin/air surface, a phenomenon related to depletion layers developed in thick porphyrin layers creating inner fields in opposite directions at the ITO/porphyrin and porphyrin/air interfaces.<sup>35,36,38,39</sup> When very thin films (about one monolayer thick) were measured in SPS, photo-induced charge transfer between porphyrins and the metal oxide electrode was noted.<sup>37–39</sup> We assume that illuminating multilayers/ITO interfaces through the transparent substrate results in differences in surface potential, measured at the porphyrin layer surface, due to photo-induced charge transfer between porphyrins and the ITO.

A change in SPV is noted under illumination at wavelength near the absorption peaks, with the SPV peaking near the absorption peak positions (Fig. 2 and S2†). A decrease in the CPD (increased SPV) was observed for all porphyrin multilayer interfaces upon illumination at wavelengths approaching 435 nm

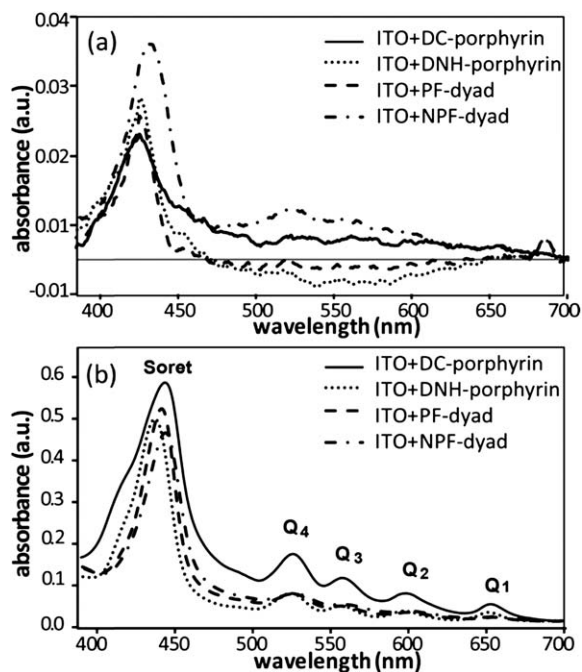


Fig. 1 Absorption spectra of porphyrin (a) monolayers and (b) multilayers on ITO substrates. The monolayer spectra were derived by subtracting the reference spectra of bare ITO from that of monolayer-modified samples. Due to inaccuracies resulting from interferences in ITO, some monolayer spectra show negative absorption where the absorption is very small.

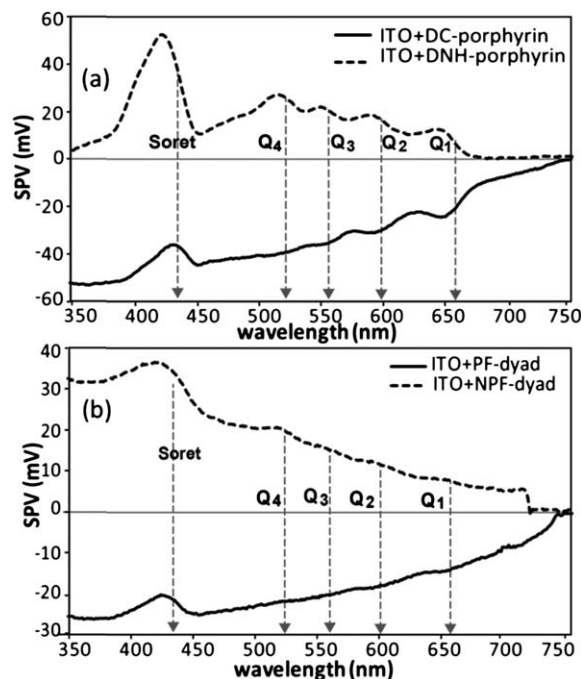
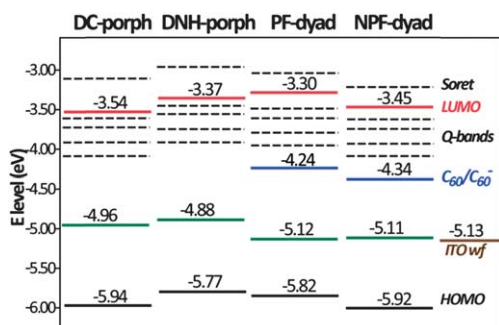


Fig. 2 SPV spectra of (a) DC- and DNH-porphyrin, and (b) PF- and NPF-dyad multilayers on ITO, showing the surface photovoltage as a function of illuminating wavelength. The arrows indicate the positions of the corresponding absorption peaks.

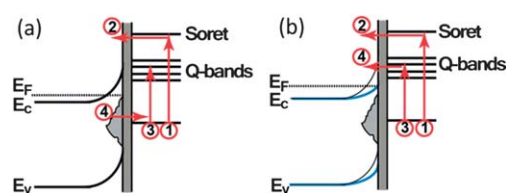
(Fig. 2), *i.e.*, approaching the Soret excitation energy. Such SPV increase indicates that Soret band absorption in all porphyrin derivatives resulted in electron injection from the molecular layer into the ITO. Upon Soret band excitation electrons are excited from the HOMO to the Soret-related level (process 1 in Scheme 3) and injected to the ITO's conduction band (process 2 in Scheme 3) due to the higher relative position of the Soret band energy level with respect to the conduction band minimum of ITO. Thus, electron injection from the Soret excited singlet state occurs faster than relaxation of this state to the lower excited state (Q-band). The ITO's conduction band edge level was deduced from the ITO's Fermi level energy which was determined experimentally (see Scheme 2). As a degenerate n-type semiconductor, the Fermi level of ITO is close to (slightly higher than) the conduction band minimum in the bulk.<sup>29,31</sup>

Four shoulders/peaks are seen in the SPV spectra between 500 and 650 nm (Fig. 2a), in agreement with the Q-band transitions (Fig. 1). Although injection of excited electrons from both porphyrins into the ITO's conduction band upon Q-band excitation was expected, from the Q-bands' energy level alignment with respect to the ITO energy levels (Scheme 2), such behaviour is not always noted. A decrease in CPD (increased SPV) upon absorption in the Q-bands of **DNH-porphyrin** films indicates photo-induced electron injection from the molecular layer into the ITO electrode as expected. However, for the **DC-porphyrin**, CPD increases (decreased SPV) upon Q-band absorption, indicating a light-induced negative charging of the molecular layer, *i.e.*, electron injection from ITO to the molecular layer (Fig. 2a). Similarly, the SPV spectra of **NPF-dyad**/ITO samples show a decrease in CPD (increased SPV) at Q-band absorption, while those of **PF-dyad**/ITO samples show an increase in CPD (decreased SPV) at Q-band absorption (Fig. 2b). It should be noted that the Q-band transitions are not as clearly resolved in the dyad SPV spectra, probably due to intramolecular photo-induced charge transfer between the porphyrin and fullerene occurring at a faster rate than electron transfer at the ITO interface.<sup>37</sup> Indeed, differential SPV spectra show the coincidence of wavelengths corresponding to transitions in the dyads' SPV with Q-band absorption peaks (Fig. S2†).

The difference in electron transfer direction between **DC-** and **DNH-porphyrins** is explained by different alignment of the Q-band energy levels with respect to the ITO's conduction band



**Scheme 2** Electron energy level diagram of the four surface modifying porphyrin derivatives deduced from cyclic voltammetry, absorption and Kelvin probe measurements. Excited state energies are marked as dashed lines. The work functions of the multilayer samples are represented in green, while that of bare ITO is marked in brown.



**Scheme 3** Schematic diagrams of (a) **DC-** and (b) **DNH-porphyrin**/ITO interface electronic levels. Arrows indicate electron excitation or transfer direction. Electron injection to ITO as a result of Soret band excitation is shown by processes 1 and 2. Positive/negative charging of the molecular layer following Q-bands excitation (process 3) is shown by process 4 in (a)/(b), respectively.

edge, which is related to differences in the ITO's surface band bending. ITO is known to have many electron energy surface states resulting in a significant surface band-bending of up to 1 eV.<sup>53</sup> The SPV measured at wavelengths shorter than *ca.* 370 nm is related to super-bandgap absorption in ITO, leading to (partial) "flattening" of the surface band bending (Fig. S3†). An increase in SPV, as seen in this case, is typical of n-type semiconductors and indicates a significant surface band bending. Upon **DNH-porphyrin** adsorption, reduced ITO band bending is noted by a smaller increase in SPV (Fig. 3 and S3†). The reduced interface band bending of the ITO upon adsorption of **DNH-porphyrin** will promote electron injection to the ITO upon excitation of the Q-bands (processes 3 and 4 in Scheme 3b). However, no such decrease in interfacial band bending is seen in **DC-porphyrin**/ITO samples; the larger band bending at the **DC-porphyrin**/ITO interface (compared to **DNH-porphyrin**/ITO interface) introduces a barrier to this process, since the conduction band edge at the surface is higher in energy than the Q-band related levels of the porphyrin (Scheme 3a). The excitation of electrons is then followed by the transfer of electrons from occupied ITO surface states into the emptied HOMO states of the excited porphyrin (processes 3 and 4 in Scheme 3a), resulting in negative charging of the molecular layer. We note that the latter process is feasible also in the former case of **DNH-porphyrin** but is unlikely to result in a net negative charge in the molecular layer due to electron injection from Q-band related levels to the ITO's conduction band. Explaining the difference in electron transfer directions upon Q-band excitations between the two porphyrins by a barrier induced by interfacial band bending assumes band bending of about 1.1 eV. 1.1 eV is the measured

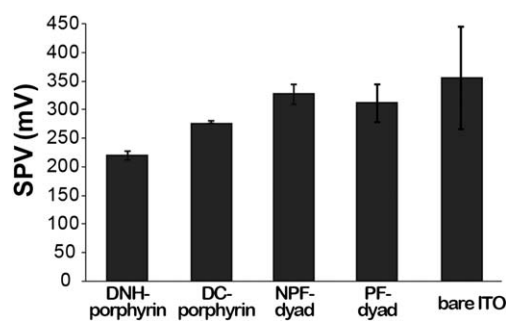


**Fig. 3** SPV of different monolayer/ITO samples upon illumination with a high intensity xenon-mercury lamp (290 W), which is proportional to the band bending at the molecular layer/ITO interface.

energy difference between the ITO's work function ( $\approx$  conduction band edge in the bulk) and the lowest Q-band level in porphyrins (see Scheme 2). Such band bending is reasonable in view of previously published values.<sup>35,53</sup> We note that explaining the differences in SPS upon Q-band illumination by opposite inner fields in the molecular multilayers<sup>35</sup> are ruled out by the almost similar Fermi level alignment in all porphyrin derivatives (Scheme 2).

As noted above, the two dyads also showed pronounced differences in their SPV spectra at the Q-band absorption range (Fig. 2b). However, no significant differences in interfacial band bending were noted between ITO modified with **PF-** and **NPF-dyads** (Fig. 3 and S3<sup>†</sup>), therefore explaining the differences in the electron transfer direction upon Q-band absorption in both dyads by an interfacial barrier is not feasible. In addition, the dyads are known to create a long-lived charge separated state under illumination,<sup>18</sup> therefore it is expected that their charge injection to/from ITO will be controlled by different mechanisms than those active in the porphyrins. Indeed, a fast transfer of electrons from the excited porphyrin states to the fullerene may diminish the transfer of such electrons to the ITO. A possible mechanism for negative surface charging upon Q-band illumination in the case of **PF-dyad** is that following photo-excitation and electron transfer to the fullerene acceptor, the porphyrin radical cations accept electrons from ITO surface states, forming a negatively charged layer, in accordance with previously published mechanisms.<sup>37,54,55</sup> The opposite behavior of **NPF-dyad** may result from its binding mode: pyridine rings are known to form hydrogen bonds between the nitrogen atom and hydroxyl protons on metal oxide surfaces.<sup>41,56,57</sup> In addition, coordinative bonding may form between the electron-withdrawing pyridine and Lewis acid sites on the ITO surface, as was demonstrated for TiO<sub>2</sub>.<sup>58</sup> We propose that this configuration, where the porphyrin moiety is located in close proximity to the ITO surface, leads to higher probability of electron injection to the ITO electrode upon Q-band excitation, which competes with electron transfer to the fullerene moiety. We note that explaining the changes in SPV measured following illumination by the formation of molecular dipoles within the dyads is unlikely as our molecular multilayers are largely disordered.

Illumination at the 500–650 nm spectral range, where porphyrin Q-band excitation occurs, is at the peak of the solar spectrum. Therefore, photoinduced electron transfer at this range is highly relevant for photovoltaic energy conversion. In porphyrin-sensitized solar cells, which typically utilize electrons injected from the porphyrins to the TiO<sub>2</sub> electrode, the opposite direction of electron transfer, as seen at **DC-porphyrin**/ITO interface, can be detrimental for the device function. Furthermore, wavelength-dependent directions of photo-induced dipoles can be utilized in wavelength-sensitive photosensors and artificial color vision. Understanding the details of photo-induced electron injection can help tailor the device function with the molecular structure.

### Porphyrins and dyads for ITO interfacial modification

Our results suggest that the first monolayer adsorbed on the surface of the ITO may determine the photo-response of multilayers adsorbed on the surface. Such behaviour may be of

significance for various optoelectronic devices. We have therefore studied the effect of the different porphyrin derivatives as interfacial modifying monolayers between multilayers of photoactive species and ITO. Multilayer films of **DME-porphyrin**, of average thickness  $40 \pm 5$  nm as estimated from AFM topography imaging, were spin cast on ITO electrodes premodified by chemically adsorbed monolayers of the four porphyrin derivatives. The **DME-porphyrin** lacks the carboxylic side groups, preventing its chemical coupling to the surface, hence it is not expected to replace the interfacial monolayer.

Fig. 4 presents the SPV spectra of those samples, compared to that of the **DME-porphyrin** multilayer on un-modified ITO. The introduction of interfacial modifying layers of porphyrin dyes was found to influence the interfacial charge transfer. The direction of the change was similar to the behaviour of the porphyrins in homogeneous multilayers (Fig. 2a and b): the introduction of **DNH-porphyrin** (Fig. 4a) and **NPF-dyad** (Fig. 4b) monolayers modified the interfacial charge transfer at the Q-band range in favour of charge injection from the photoactive molecular layer to the ITO electrode. **DC-porphyrin** interfacial monolayers had a negligible effect on the interfacial charge transport (Fig. 4a), however, a **PF-dyad** monolayer increased the charge injection from ITO to the photoactive layer upon Q-band excitation (Fig. 4b). Similar results were obtained with another non-adsorbing porphyrin derivative (**TMP-porphyrin**) as a photoactive multilayer film (Fig. S4<sup>†</sup>). The results suggest that porphyrin monolayers can act as modifying interfacial layers between photo-active layers and ITO electrodes in a predictable manner. Although light absorption and charge generation occur largely in the photoactive multilayer film, the

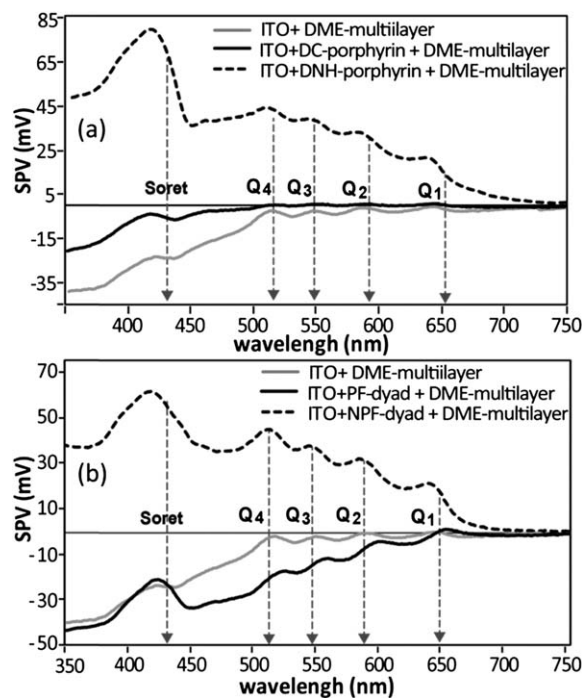


**Fig. 4** SPV spectra of **DME-porphyrin** multilayers adsorbed on ITO modified with (a) **DC-** and **DNH-porphyrin** monolayers, and (b) **PF-** and **NPF-dyad** monolayers. The arrows indicate the positions of the corresponding absorption peaks in the **DME-porphyrin** absorption spectrum.

interfacial chemistry, determined by the chemically adsorbed photoactive monolayer, significantly affects the photo-induced charge transfer efficiency at the interface.

## Summary and conclusions

This work has shown that changing the porphyrin peripheral substituents can affect the direction of interfacial charge transfer at porphyrin/ITO interfaces. Soret-band excitation resulted in electron injection from the molecular layer to the ITO in all porphyrin derivatives, suggesting that electron injection is faster than relaxation from the porphyrin upper excited state to the lower one. Adsorption of **DNH-porphyrin** was shown to induce a smaller ITO surface band bending, which favoured the injection of Q-band excited electron from the porphyrin layer to the ITO conduction band. In contrast, **DC-porphyrin** adsorption resulted in electron transfer from the ITO to the molecular layer upon Q-band excitation, while the opposite direction of electron transfer was blocked by a barrier formed by the relatively large band bending at the ITO surface. Similar differences in the direction of electron injection following Q-band excitation were noted in porphyrin–fullerene dyads differing by a pyridine end group. This difference was explained by the dyads' different adsorption configurations on the ITO surface. The pyridine ring attached to the porphyrin moiety in **NPF-dyads** is proposed to act as an electron-accepting anchoring group, enhancing photo-induced charge injection into the ITO conduction band at the expense of intramolecular electron transfer to the fullerene moiety. This photo-induced charge injection in the 500–650 nm spectral range (Q-band excitation in porphyrins) is highly relevant for photovoltaic devices, as the solar spectrum peaks in this range.

The charge transfer behaviour was shown to depend on the chemical nature of the first monolayer adsorbed on the surface. We propose that modified porphyrin derivatives can be used for the modification of interfacial charge transfer at ITO/photoactive organic layer interfaces in a predefined, controllable way. The relationships between porphyrin substituents and interfacial optoelectronic properties presented in this work could be utilized for fabrication of improved organic optoelectronic devices.

## Experimental

### Materials

Solvents were purchased from Bio-Lab, Fluka, D-chem and Acros Organics Chemicals (all “absolute grade”, HPLC analyzed) and were used without further purification. 5-Mesityldipyrrromethane (95%) was purchased from Frontier Scientific, USA. 4-Formylbenzoate (99%), *p*-chloranil, 2,4-dinitrochlorobenzene ( $\geq 98\%$ ), hydrazine monohydrate (98%) and pyridine (99.8%) were purchased from Sigma-Aldrich. 3,4,5-Trimethoxy benzylamine (98%) was purchased from D-chem, Israel. All chemicals were used as received without further purification.

### Synthesis

Synthesis of different meso-substituted porphyrins was carried out based on previously reported procedures.<sup>59</sup> The purity of

compounds and molecular structures was established by TLC, mass- and <sup>1</sup>H-NMR-spectroscopies. The NMR spectra were recorded using a Bruker Avance DMX500 spectrometer. Mass spectra were measured by a Bruker Daltonics Reflex IV Matrix-Assisted Laser Desorption Ionization Time-Of-Flight (MALDI-TOF) instrument.

### DME-porphyrin

A solution of 5-mesityldipyrrromethane (264 mg, 1 mmol) and methyl 4-formylbenzoate (164 mg, 1 mmol) in 300 ml CH<sub>2</sub>Cl<sub>2</sub> was degassed by bubbling with nitrogen for 30 min. The reaction mixture was shielded from ambient light and treated with trifluoric acid (150  $\mu$ l) at room temperature.<sup>60</sup> After stirring for 40 min under a N<sub>2</sub> atmosphere, *p*-chloranil (490 mg, 2 mmol) was added and the reaction mixture was stirred for an additional 1 h. Triethylamine (1 ml) was added, and the solvent was evaporated. The resulting solid crude was purified by silica gel chromatography (ethyl acetate/petroleum ether (b.p. 60–80 °C) = 0/1  $\rightarrow$  1/0). The resulting residue was washed with acetonitrile, filtered and dried under vacuum, producing a pure **DME-porphyrin** compound (135 mg, 0.165 mmol, 33% yield). <sup>1</sup>H NMR (200 MHz, CDCl<sub>3</sub>) p.p.m.:  $\delta$  1.84 (s, 12H), 2.64 (s, 6H), 4.12 (s, 6H), 7.21 (s, 4H), 8.29–8.46 (dd, 8H), 8.70–8.76 (m, 8H). MS (MALDI-TOF) 815.0, calc. 815.2.

### DC-porphyrin

A mixture of **DME-porphyrin** (135 mg, 0.165 mmol) in 100 ml of dioxane and 1 N NaOH (10 ml) was refluxed for 6 h. After cooling, acidification with 1 N HCl and subsequent filtration produced **DC-porphyrin** as a vivid reddish purple powder (124 mg, 0.156 mmol, 95% yield). <sup>1</sup>H NMR (500 MHz, d<sub>6</sub>-DMSO) p.p.m.:  $\delta$  1.75 (s, 12H), 2.56 (s, 6H), 7.34 (s, 4H), 8.35 (m, 8H), 8.63–8.81 (dd, 8H); MS (MALDI-TOF) 787.4, calc. 786.9.

### DNH-porphyrin

2,4-Dinitrophenyl hydrazine synthesis: 2,4-dinitrochlorobenzene (1.50 g, 7.4 mmol) was dissolved in 50 ml of ethanol and the resulting solution was added dropwise to a solution of 5 ml of hydrazine monohydrate in 50 ml ethanol for 30 min. The reaction mixture was refluxed with stirring for 3 h. Brine was added and the crystalline solid was filtered and dried (1.34 g, 6.8 mmol, 91% yield): m.p. 198–202°; <sup>1</sup>H NMR (200 MHz, CDCl<sub>3</sub>) p.p.m.:  $\delta$  4.0 (s, 2H), 7.83–7.88 (d, 1H), 8.28–8.29 (d, 1H), 9.10–9.12 (d, 1H), 9.44 (s, 1H).

**DC-porphyrin** (124 mg, 0.156 mmol) was added to a solution of 2 ml thionyl chloride in 50 ml toluene and refluxed for 6 h. After cooling, the solvent was evaporated and the solid crude (bis(acyl chloride)-porphyrin) was dissolved in 20 ml of toluene and used in the next stage without purification. The solution of activated porphyrin (10 ml, 0.08 mmol) was added to a solution of 2,4-dinitrophenyl hydrazine (10 mg, 0.05 mmol) in 2 ml of dry pyridine. The reaction mixture was stirred for 5 h at room temperature and then poured into 1 N HCl solution (100 ml). The product was extracted with ethyl acetate (100 ml), washed with water several times and dried over anhydrous Na<sub>2</sub>SO<sub>4</sub>. The resulting solid crude product was purified by silica gel chromatography (ethyl acetate/petroleum ether = 0/1  $\rightarrow$  1/0). A mixture

of the two compounds with one or two 2,4-dinitrophenyl hydrazine substituent was obtained (TLC silica, ethyl acetate : petroleum ether = 1 : 1) and was further separated by additional silica gel chromatography (ethyl acetate/petroleum ether = 0/1 → 1/0). The desired compound was obtained in 15% yield (11.6 mg): <sup>1</sup>H NMR (500 MHz, d6) p.p.m.: δ -2.51 (s, 2H), 1.85 (s, 12H), 2.63 (s, 6H), 7.365 (s, 4H), 7.82–7.84 (d, 1H), 8.38–8.40 (m, 1H), 8.44–8.52 (m, 8H), 8.76–8.88 (dd, 8H), 9.13 (d, 1H), 10.26 (s, 1H), 10.70 (s, 1H); MS (MALDI-TOF) 966.9, calc. 967.

### TMP-porphyrin

**DC-porphyrin** (124 mg, 0.156 mmol) was added to a solution of 2 ml thionyl chloride in 50 ml toluene and refluxed for 6 h. After cooling, the solvent was evaporated and the solid crude (bis(acyl chloride)-porphyrin) was dissolved in 20 ml of toluene and used in the next stage without purification. The solution of activated porphyrin (10 ml, 0.08 mmol) was added to a solution of 3,4,5-trimethoxy benzylamine (40 mg, 0.2 mmol) in 2 ml of dry pyridine. The reaction mixture was stirred for 5 h at room temperature and then poured into 1 N HCl solution (100 ml). The product was extracted with ethyl acetate (100 ml), washed with water several times and dried over anhydrous Na<sub>2</sub>SO<sub>4</sub>. The resulting solid crude product was partially purified by silica gel chromatography (ethyl acetate/petroleum ether = 0/1 → 1/0). The resulting mixture was further separated by additional silica gel chromatography (ethyl acetate/petroleum ether = 0/1 → 1/0). The desired compound was obtained at 22% yield (20.2 mg): <sup>1</sup>H-NMR (500 MHz, d6) p.p.m.; MS (MALDI-TOF) 1144.7, calc. 1145.

### PF- and NPF-dyads

The porphyrin–fullerene dyads were synthesized by Prof. Devens Gust group *via* previously reported synthetic procedures.<sup>61</sup>

### Sample preparation

Pure mono- and multi-layers of porphyrin derivatives were prepared on ITO thin films (80–100 nm thick) with nominal sheet resistance 20–25 Ω sq<sup>-1</sup>, deposited on SiO<sub>2</sub> passivated float glass substrates (Delta Technologies). The substrates were cleaned using freshly prepared piranha solution (4 : 2 vol ratio concentrated H<sub>2</sub>SO<sub>4</sub> and 30 vol% H<sub>2</sub>O<sub>2</sub>) for 40 min followed by washing with deionized water (18.2 MΩ cm) and drying under nitrogen stream (**Caution: Piranha is a very strong oxidant and reacts violently with many organic materials**). Cleaned substrates were immersed in dye solution overnight (12–24 h) for adsorption *via* carboxylic acid substituents. **PF-** and **NPF-dyads** were adsorbed from chloroform solutions (0.5 mM); **DNH-porphyrin** from a toluene solution (0.5 mM); and **DC-porphyrin** from a tetrahydrofuran (THF) solution (2 mM). Multilayer samples of the chemically adsorbing porphyrin derivatives were prepared by removal of electrodes from the dye solution and subsequent solvent evaporation under a weak nitrogen stream without washing. Monolayer samples were prepared by removal of the substrates from the dye solutions followed by thorough rinsing in their appropriate solvents. Physically adsorbed multilayer samples were prepared by spin casting from a 13 mM solution of **DME-porphyrin** or **TMP-porphyrin** in THF and chloroform,

respectively, at 2000 rpm. All samples were stored in nitrogen ambient in the dark after preparation and between measurements.

### Surface photovoltage spectroscopy measurements

In SPS, the surface photovoltage is measured as a function of the illuminating wavelength, providing information on the energetics of the surface or interface under study. Light induced charge transfer between the ITO substrate electrode and an adsorbed molecular layer results in dipole formation which is expressed in the contact potential difference (CPD) measured between the ITO surface and a Kelvin probe (CPD = sample work function – probe work function). The changes in CPD were measured by the Kelvin probe technique using a reference gold electrode (Besocke Deltha Phi, Germany). The measurements were conducted at room temperature and in a nitrogen-rich ambient environment (~14% humidity). The samples were placed in a fully darkened Faraday cage and the CPD was followed until it reached a constant value (±1 mV) before illumination was turned on. For SPS, the CPD signal was monitored as a function of photon energy. The illumination was provided by a 350 W xenon–mercury light source (Oriel Inc., USA) and passed through a double monochromator, model MS257 (Oriel Inc., USA). The illumination intensity was in the range 10–50 μW cm<sup>-2</sup>, with wavelength intervals of 1 nm and duration of 2 s per interval. The samples were illuminated through the transparent substrate.

### Complementary molecular layer characterization

UV/VIS absorption measurements were carried out using a JASCO V-570 UV/VIS/NIR spectrophotometer. Topographical imaging of surface morphology was obtained by AFM (Solver-Pro, NTMDT, Russia) in semi-contact mode, using the noncontact tip Multi75Al-G (3 N m<sup>-1</sup> – 75 kHz; Budget Sensors). Cyclic voltammetry measurements were performed using a three-electrode potentiostat (VersaSTAT4, Princeton Applied Research). The measurements were carried out in dried, distilled dichloromethane solution containing 0.10 M tetra-*n*-butylammonium hexafluorophosphate supporting electrolyte using a glassy carbon working electrode (CH Instruments, Inc.), electrode area 0.07 cm<sup>2</sup>, a platinum wire as a counter electrode, and a Ag/Ag<sup>+</sup> quasi-reference electrode, with a sweep rate of 0.1 V s<sup>-1</sup>. The measurements were performed at room temperature under N<sub>2</sub>. The potentials were reported *vs.* the ferrocene/ferrocenium (Fe/Fe<sup>+</sup>) internal reference couple, whose redox potential *vs.* Ag/Ag<sup>+</sup> was 0.2 V.

### Acknowledgements

This research was supported by a BSF grant #2008340. The authors thank Dr A. Aizikovitch for help with the synthesis. YF thanks the Jacques Lewiner Chemistry Department Scholarship and BGU Internal Interdisciplinary Research fellowship for financial support. This work was supported in part by a grant from the U. S. Department of Energy (DE-FG02-03ER15393).

### References

- 1 N. S. Lewis, *Science*, 2007, **315**, 798–801.

- 2 B. Kippelen and J.-L. Bredas, *Energy Environ. Sci.*, 2009, **2**, 251–261.
- 3 H. Hoppe and N. S. Sariciftci, *J. Mater. Res.*, 2004, **19**, 1924–1945.
- 4 D. Cahen, A. Kahn and E. Umbach, *Mater. Today*, 2005, **8**, 32–41.
- 5 G. Ashkenasy, D. Cahen, R. Cohen, A. Shanzer and A. Vilan, *Acc. Chem. Res.*, 2002, **35**, 121–128.
- 6 A. Vilan and D. Cahen, *Trends Biotechnol.*, 2002, **20**, 22–29.
- 7 L. Zuppiroli, L. Si-Ahmed, K. Kamaras, F. Nuesch, M. N. Bussac, D. Ades, A. Siove, E. Moons and M. Grätzel, *Eur. Phys. J. B*, 1999, **11**, 505–512.
- 8 S. K. Hau, H. Yip, O. Acton, N. S. Baek, H. Ma and A. K. Jen, *J. Mater. Chem.*, 2008, **18**, 5113–5119.
- 9 E. L. Ratcliff, B. Zacher and N. R. Armstrong, *J. Phys. Chem. Lett.*, 2011, **2**, 1337–1350.
- 10 E. D. Gomez and Y. Loo, *J. Mater. Chem.*, 2010, **20**, 6604–6611.
- 11 S. Park, T. U. Kampen, D. R. T. Zahn and W. Braun, *Appl. Phys. Lett.*, 2001, **79**, 4124–4126.
- 12 R. Cohen, S. Bastide, D. Cahen, J. Libman, A. Shanzer and Y. Rosenwaks, *Opt. Mater.*, 1998, **9**, 394–400.
- 13 R. Cohen, L. Kronik, A. Shanzer, D. Cahen, A. Liu, Y. Rosenwaks, J. K. Lorenz and A. B. Ellis, *J. Am. Chem. Soc.*, 1999, **121**, 10545–10553.
- 14 C. Goh, S. R. Scully and M. D. McGehee, *J. Appl. Phys.*, 2007, **101**, 114503.
- 15 Y. Huang, J. Hsu, Y. Liao, W. Yen, S. Li, S. Lin, C. Chen and W. Su, *J. Mater. Chem.*, 2011, **21**, 4450–4456.
- 16 Y. Lin, T. Chu, S. Li, C. Chuang, C. Chang, W. Su, C. Chang, M. Chu and C. Chen, *J. Am. Chem. Soc.*, 2009, **131**, 3644–3649.
- 17 W. Zhang, R. Zhu, B. Liu and S. Ramakrishna, *Appl. Energy*, 2012, **90**, 305–308.
- 18 D. Gust, T. A. Moore and A. L. Moore, *Acc. Chem. Res.*, 2001, **34**, 40–48.
- 19 D. Gust, T. A. Moore and A. L. Moore, *Acc. Chem. Res.*, 1993, **26**, 198–205.
- 20 W. M. Campbell, A. K. Burrell, D. L. Officer and K. W. Jolley, *Coord. Chem. Rev.*, 2004, **248**, 1363–1379.
- 21 M. V. Martinez-Diaz, G. de la Torre and T. Torres, *Chem. Commun.*, 2010, **46**, 7090–7108.
- 22 C. Hsieh, H. Lu, C. Chiu, C. Lee, S. Chuang, C. Mai, W. Yen, S. Hsu, E. W. Diau and C. Yeh, *J. Mater. Chem.*, 2010, **20**, 1127–1134.
- 23 K. Yamashita, Y. Harima and T. Matsubayashi, *J. Phys. Chem.*, 1989, **93**, 5311–5315.
- 24 T. Bessho, S. M. Zakeeruddin, C. Yeh, E. W. Diau and M. Grätzel, *Angew. Chem., Int. Ed.*, 2010, **49**, 6646–6649.
- 25 C. Hsieh, H. Lu, C. Chiu, C. Lee, S. Chuang, C. Mai, W. Yen, S. Hsu, E. W. Diau and C. Yeh, *J. Mater. Chem.*, 2010, **20**, 1127–1134.
- 26 S. Dos Tracy, A. Morandeira, S. Koops, A. J. Mozer, G. Tsekouras, Y. Dong, P. Wagner, G. Wallace, J. C. Earles, K. C. Gordon, D. Officer and J. R. Durrant, *J. Phys. Chem. C*, 2010, **114**, 3276–3279.
- 27 C. Lee, H. Lu, C. Lan, Y. Huang, Y. Liang, W. Yen, Y. Liu, Y. Lin, R. W. Diau and C. Yeh, *Chem.–Eur. J.*, 2009, **15**, 1403–1412.
- 28 C. Lin, C. Lo, L. Luo, H. Lu, C. Hung and E. W. Diau, *J. Phys. Chem. C*, 2009, **113**, 755–764.
- 29 Y. Gassenbauer, R. Schafranek, A. Klein, S. Zafeiratos, M. Havecker, A. Knop-Gericke and R. Schlogl, *Phys. Rev. B: Condens. Matter Mater. Phys.*, 2006, **73**, 245312.
- 30 C. Korber, V. Krishnakumar, A. Klein, G. Panaccione, P. Torelli, A. Walsh, J. L. F. Da Silva, S.-H. Wei, R. G. Egdell and D. J. Payne, *Phys. Rev. B: Condens. Matter Mater. Phys.*, 2010, **81**, 165207.
- 31 Y. Gassenbauer and A. Klein, *J. Phys. Chem. B*, 2006, **110**, 4793–4801.
- 32 E. L. Hanson, J. Guo, N. Koch, J. Schwartz and S. L. Bernasek, *J. Am. Chem. Soc.*, 2005, **127**, 10058–10062.
- 33 C. Ganzorig, K. Kwak, K. Yagi and M. Fujihira, *Appl. Phys. Lett.*, 2001, **79**, 272–274.
- 34 Y. Vaynzof, D. Kabra, L. Zhao, P. K. H. Ho, A. T. S. Wee and R. H. Friend, *Appl. Phys. Lett.*, 2010, **97**, 033309.
- 35 E. Moons, A. Goossens and T. Savenije, *J. Phys. Chem. B*, 1997, **101**, 8492–8498.
- 36 Y. Zidon, Y. Shapira and T. Dittrich, *J. Appl. Phys.*, 2007, **102**, 053705.
- 37 F. Fungo, M. E. Milanesio, E. N. Durantini, L. Otero and T. Dittrich, *J. Mater. Chem.*, 2007, **17**, 2107–2112.
- 38 Q. Zhao, M. Yu, T. Xie, L. Peng, P. Wang and D. Wang, *Nanotechnology*, 2008, **19**, 245706.
- 39 P. Zabel, T. Dittrich, M. Funes, E. N. Durantini and L. Otero, *J. Phys. Chem. C*, 2009, **113**, 21090–21096.
- 40 S. A. Vail, D. I. Schuster, D. M. Guldi, M. Isosomppi, N. Tkachenko, H. Lemmetyinen, A. Palkar, L. Echegoyen, X. Chen and J. Z. H. Zhang, *J. Phys. Chem. B*, 2006, **110**, 14155–14166.
- 41 Y. Ooyama, S. Inoue, R. Asada, G. Ito, K. Kushimoto, K. Komaguchi, I. Imae and Y. Harima, *Eur. J. Org. Chem.*, 2010, **2010**, 92–100.
- 42 H. Imahori, M. Kimura, K. Hosomizu and S. Fukuzumi, *J. Photochem. Photobiol., A*, 2004, **166**, 57–62.
- 43 H. Imahori, H. Norieda, H. Yamada, Y. Nishimura, I. Yamazaki, Y. Sakata and S. Fukuzumi, *J. Am. Chem. Soc.*, 2001, **123**, 100–110.
- 44 J. L. McHale, *J. Phys. Chem. Lett.*, 2012, **3**, 587–597.
- 45 F. Fungo, L. Otero, C. D. Borsarelli, E. N. Durantini, J. J. Silber and L. Sereno, *J. Phys. Chem. B*, 2002, **106**, 4070–4078.
- 46 H. N. Fonda, J. V. Gilbert, R. A. Cormier, J. R. Sprague, K. Kamioka and J. S. Connolly, *J. Phys. Chem.*, 1993, **97**, 7024–7033.
- 47 D. I. Schuster, P. Cheng, P. D. Jarowski, D. M. Guldi, C. Luo, L. Echegoyen, S. Pyo, A. R. Holzwarth, S. E. Braslavsky, R. M. Williams and G. Klihm, *J. Am. Chem. Soc.*, 2004, **126**, 7257–7270.
- 48 C. M. Cardona, W. Li, A. E. Kaifer, D. Stockdale and G. C. Bazan, *Adv. Mater.*, 2011, **23**, 2367–2371.
- 49 D. P. Hagberg, J. Yum, H. Lee, F. De Angelis, T. Marinado, K. M. Karlsson, R. Humphry-Baker, L. Sun, A. Hagfeldt, M. Graetzel and M. K. Nazeeruddin, *J. Am. Chem. Soc.*, 2008, **130**, 6259–6266.
- 50 J. K. Park, H. R. Lee, J. Chen, H. Shinokubo, A. Osuka and D. Kim, *J. Phys. Chem. C*, 2008, **112**, 16691–16699.
- 51 L. Kronik and Y. Shapira, *Surf. Interface Anal.*, 2001, **31**, 954–965.
- 52 M. Eschle, E. Moons and M. Graetzel, *Opt. Mater.*, 1998, **9**, 138–144.
- 53 A. Klein, *Appl. Phys. Lett.*, 2000, **77**, 2009–2011.
- 54 T. Vuorinen, K. Kaunisto, N. V. Tkachenko, A. Efimov, H. Lemmetyinen, A. S. Alekseev, K. Hosomizu and H. Imahori, *Langmuir*, 2005, **21**, 5383–5390.
- 55 T. Vuorinen, K. Kaunisto, N. V. Tkachenko, A. Efimov and H. Lemmetyinen, *J. Photochem. Photobiol., A*, 2006, **178**, 185–191.
- 56 T. J. Dines, L. D. MacGregor and C. H. Rochester, *Spectrochim. Acta, Part A*, 2003, **59**, 3205–3217.
- 57 M. I. Zaki, M. A. Hasan, F. A. Al-Sagheer and L. Pasupulety, *Colloids Surf., A*, 2001, **190**, 261–274.
- 58 Y. Ooyama, S. Inoue, T. Nagano, K. Kushimoto, J. Ohshita, I. Imae, K. Komaguchi and Y. Harima, *Angew. Chem., Int. Ed.*, 2011, **50**, 7429–7433.
- 59 J. S. Lindsey, *Acc. Chem. Res.*, 2010, **43**, 300–311.
- 60 C. M. Carcel, J. K. Laha, R. S. Loewe, P. Thamyongkit, K. Schweikart, V. Misra, D. F. Bocian and J. S. Lindsey, *J. Org. Chem.*, 2004, **69**, 6739–6750.
- 61 S. Battacharyya, A. Kibel, G. Kodis, P. A. Liddell, M. Gervaldo, D. Gust and S. Lindsay, *Nano Lett.*, 2011, **11**, 2709–2714.